JBC EDITORS' PICK

Direct relationship between increased expression and mistrafficking of the Charcot–Marie–Tooth–associated protein PMP22

Received for publication, June 22, 2020, and in revised form, June 30, 2020 Published, Papers in Press, July 9, 2020, DOI 10.1074/jbc.AC120.014940

Justin T. Marinko[1,2], **Bruce D. Carter**[1,3], **and Charles R. Sanders**[1,2,4,*]

From the [1]*Department of Biochemistry and the* [2]*Center for Structural Biology, Vanderbilt University, Nashville, Tennessee, USA, the* [3]*Vanderbilt Brain Institute, Nashville, Tennessee, USA, and the* [4]*Department of Medicine, Vanderbilt University Medical Center, Nashville, Tennessee, USA*

Edited by Karen G. Fleming

Charcot–Marie–Tooth disease (CMT) is a neuropathy of the peripheral nervous system that afflicts ~1:2500 people. The most common form of this disease (CMT1A, 1:4000) is associated with duplication of chromosome fragment 17p11.2-12, which results in a third WT *PMP22* allele. In rodent models overexpressing the PMP22 (peripheral myelin protein 22) protein and in dermal fibroblasts from patients with CMT1A, PMP22 aggregates have been observed. This suggests that overexpression of PMP22 under CMT1A conditions overwhelms the endoplasmic reticulum quality control system, leading to formation of cytotoxic aggregates. In this work, we used a single-cell flow-cytometry trafficking assay to quantitatively examine the relationship between PMP22 expression and trafficking efficiency in individual cells. We observed that as expression of WT or disease variants of PMP22 is increased, the amount of intracellular PMP22 increases to a greater extent than the amount of surface-trafficked protein. This was true for both transiently transfected cells and PMP22 stable expressing cells. Our results support the notion that overexpression of PMP22 in CMT1A leads to a disproportionate increase in misfolding and mistrafficking of PMP22, which is likely a contributor to disease pathology and progression.

Charcot–Marie–Tooth disease (CMT) is an eponym for a large range of related neuropathies that occur with a prevalence of ~1:2500 in the human population (1, 2). Patients with CMT suffer from a range of symptoms including impaired tendon reflexes, weakness of the distal musculature, abnormalities of the peripheral nerve axon and its adjacent myelin sheath, and, in severe cases, confinement to a wheelchair (1, 3–5). Over two-thirds of CMT cases result from mutations in the *PMP22* gene, including the most common form of the disease, CMT1A (6). CMT1A is linked to a heterozygous duplication of chromosome fragment 17p11.2-12, resulting in the production of a third copy of the *PMP22* allele (trisomy). Although nine other proteins are also overexpressed in this process, it has been shown that CMT1A is caused by the additional copy of *PMP22* (1, 2, 7). Whether the disease arises from an absolute increase in protein expression or resulting fluctuations in levels of PMP22 is up for debate; however, it is clear that increasing the copy number of *PMP22* in rodents results in pathological phenotypes similar to those observed in patients with CMT1A (7–9). Deletion of a *PMP22* allele (*WT/null* conditions) and genetically dominant point mutations in PMP22 also result in forms of CMT (1, 6).

PMP22 encodes a tetraspan integral membrane protein, PMP22, comprising 2–5% of the protein content in compact myelin of the peripheral nervous system (10, 11). The specific biological functions of PMP22 are still under investigation; however, substantial evidence suggests that it plays a structural role in the maintenance and development of compact myelin (1). Indeed, when PMP22 is reconstituted into lipid bilayers, it is sufficient to induce wrapping of the membranes to produce myelin-like assemblies (12). However, PMP22 has also been implicated in a number of other processes within myelin-producing Schwann cells (1, 2, 13–16). *In vitro* studies revealed that PMP22 is only modestly stable in detergent micelles, with the native conformation favored over the denatured ensemble by only 1.5 ± 0.1 kcal mol^{-1} (17, 18). That the folded form is marginally stable appears to be directly related to why only ~20% of synthesized WT protein is able to fully mature and traffic to the plasma membrane (PM) (17, 19, 20).

Why a third copy of *PMP22* results in neuropathy is not clearly established. Patients afflicted with CMT1A present slowed nerve conduction velocity and axonal loss, accompanied by a shortening of internodal length (1). Beyond these morphological changes in compact myelin, overexpression of PMP22 has also been shown to cause Schwann cell apoptosis (21, 22). Mouse models with multiple copies of WT *PMP22* or expressing disease mutant forms of PMP22, as well as CMT1A patient-derived dermal fibroblasts, display the presence of cytosolic PMP22 aggregates coinciding with a decrease in proteasomal activity (1, 8, 13, 23, 24). Under normal conditions, PMP22 that is not able to mature beyond the endoplasmic reticulum (ER) is removed from the membrane by ER quality control and degraded in the cytosol via proteosomal and/or lysosomal pathways (23). One hypothesis for CMT1A pathology is that under normal conditions, expression of *PMP22* occurs at levels that approach saturation of the ER protein folding quality control system, such that introduction of a third copy of *PMP22* overwhelms the system, leading to ER stress and accumulation of cytotoxic aggregates. This is supported by the fact that stimulation of autophagy leads to increased degradation of such

This article contains supporting information.

* For correspondence: Charles R. Sanders, chuck.sanders@vanderbilt.edu.

aggregates and improved myelination in cultures and in mice (25, 26). In this work, we quantitatively examine the question of whether increased expression of PMP22 in model cell lines results in increased formation of intracellularly trapped protein and a decrease in PM trafficking efficiency.

Results

Measurement of PMP22 trafficking efficiency

For this study we used a previously described single-cell flow cytometry-based assay that quantitates the levels of both PM and intracellular PMP22 (17). Because the fusion of fluorescent reporter proteins to PMP22 has been shown to cause intracellular retention and aggregation, we inserted a c-myc epitope tag into the second extracellular loop of the protein (Fig. 1*A*). This modification has been shown not to affect protein function or turnover (17, 27). In our experimental workflow (Fig. S1), PMP22-expressing cells are harvested and fixed followed by incubation with a myc antibody conjugated to phycoerythrin, which labels surface-expressed PMP22 (properly trafficked, mature PMP22). Following a wash step, the cells were permeabilized and internal PMP22 (misfolded PMP22 plus a likely small population of actively folding/trafficking protein) was labeled with the same anti-myc antibody but this time conjugated to Alexa Fluor 647. Surface and internal concentrations of PMP22 in single cells were then quantified using flow cytometry with fluorimetric detection. Fluorescent intensities of the two fluorophores were normalized by fixing and permeabilizing a population of PMP22-expressing cells, splitting the population in two, and labeling each half with only one antibody.

This experimental setup was used to measure WT PMP22 trafficking efficiency in transiently transfected HEK293 cells. We define trafficking efficiency as the fraction of PMP22 localized to the PM compared with the total PMP22 in the cell (PM intensity/(PM intensity + internal intensity)). Efficiency can vary from 0.0 (all PMP22 is intracellular) to 1.0 (all PMP22 is found at the PM). In three biological replicates, interrogating 2500 individual HEK293 cells per experiment, we found that WT PMP22 traffics to the PM with a mean trafficking efficiency of 0.27 ± 0.01 (mean ± 95% confidence interval; Fig. 1*B*).

We pooled the 7500 cells and binned them according to their trafficking efficiencies in bin sizes of 0.04 efficiency units (Fig. 1*B*). A population analysis of the cells revealed a left-skewed Gaussian distribution centered ~0.2, corresponding with previously measured PMP22 trafficking efficiencies. We also reanalyzed previously reported data collected using the same experimental setup in Madin–Darby canine kidney (MDCK) cells (17). As shown in Fig. 1*C*, we observed a similar population distribution of trafficking efficiencies, but the curve is left-shifted relative to HEK293, and the mean trafficking efficiency (0.17 ± 0.03) is lower.

WT PMP22 trafficking efficiency as a function of total expression

Normalized, background-corrected, total relative fluorescent intensity (RFU) of PMP22, corresponding to total cellular PMP22, ranged from roughly 50 to 125,000 RFU in individual

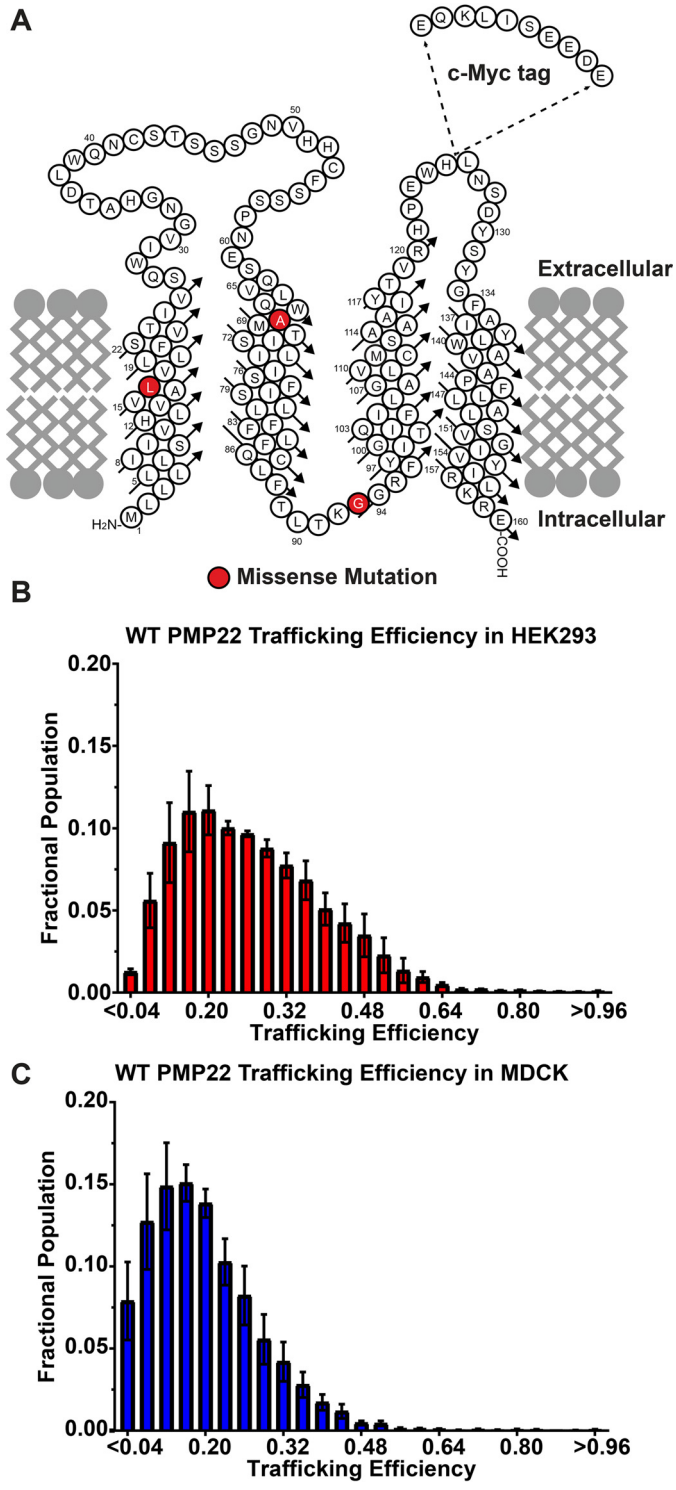

Figure 1. *A*, cartoon topology diagram of PMP22 in a membrane. The c-myc tag is shown where it was inserted into the sequence. Disease variant sites for mutants examined in this study are highlighted in *red*. *B* and *C*, population distribution of WT PMP22 trafficking efficiency measured in individual transiently transfected HEK293 cells (*B*) or in MDCK cells (*C*), each from three independent biological experiments with 2500 cells measured per replicate. Fractional populations for each bin were calculated for each replicate, and the means ± S.E. are shown. The data for *C* was obtained by reanalyzing a data set originally reported in Ref. 17.

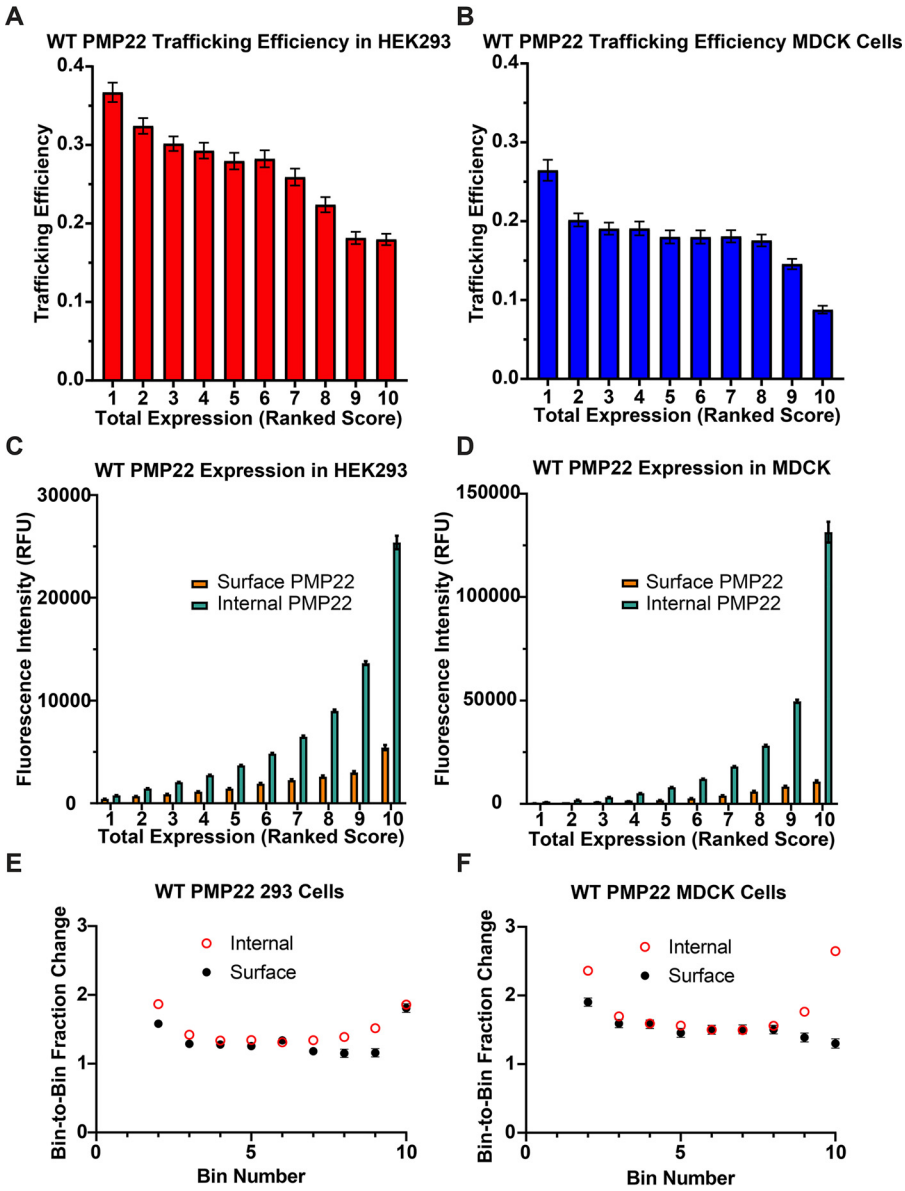

Figure 2. WT PMP22 trafficking efficiency in individual cells *versus* total PMP22 expression. *A* and *B*, PMP22 trafficking efficiency was measured for each of 7500 individual transiently transfected HEK293 cells (*A*) or transiently transfected MDCK cells (*B*), each from three independent biological replicates. The cells were placed into 10 bins representing 750 cells each based on total PMP22 expression. The mean trafficking efficiency ± 95% CI is plotted for each bin. The data for *B* were obtained from a data set originally reported in Ref. 17. *C* and *D*, trafficking efficiency values plotted in *A* and *B* were deconvoluted, and the mean levels of cell surface PMP22 (*orange*) and of internal PMP22 (*green*) ± 95% CI are plotted for each bin. *E* and *F*, the fraction change of relative fluorescence between each bin (bin 2/bin1, bin 3/bin2 . . . bin10/bin 9) was calculated for both cell surface (*black circles*) and internal (*open red circles*) PMP22 shown in *C* and *D*. Mean fraction change is reported ± 95% CI (for values with no visible *error bars*, the error was too small to be represented).

HEK293 cells. In Fig. 2*A*, we grouped measurements into 10 equal-sized bins (750 cells/bin) based on total single-cell expression of PMP22 and plotted mean trafficking efficiency in each bin (for mean PMP22 expression in each bin see Fig. S2*A*). We observed a concentration dependence wherein increased expression leads to decreased trafficking efficiency. These data are interesting in light of the common CMT1A phenotype in which overexpression of PMP22 causes disease. To ensure that this observation was not cell line–dependent, we performed the same analysis on data from MDCK cells (17). MDCK cells also displayed decreased PMP22 trafficking efficiency at high total expression levels (Fig. 2*B*).

We next deconvoluted our data to examine the concentration dependence of PM and intracellular populations of PMP22. For both cell lines, as the amount of total PMP22 increases, both internal and PM PMP22 increases (Fig. 2, *C* and *D*). Fig. 2 (*E* and *F*) quantitates the bin-to-bin changes in internal and surface PMP22. For both HEK293 and MDCK cells, there is an initial (bin 1 to bin 2) jump in internal protein, followed by a plateau of steady increase in which the bin-to-bin growth rate (measured as the fraction of mean protein expression in the two bins) is the same for both internal and surface PMP22 population. The growth of the internal PMP22 population increases at higher total expression levels, with the growth

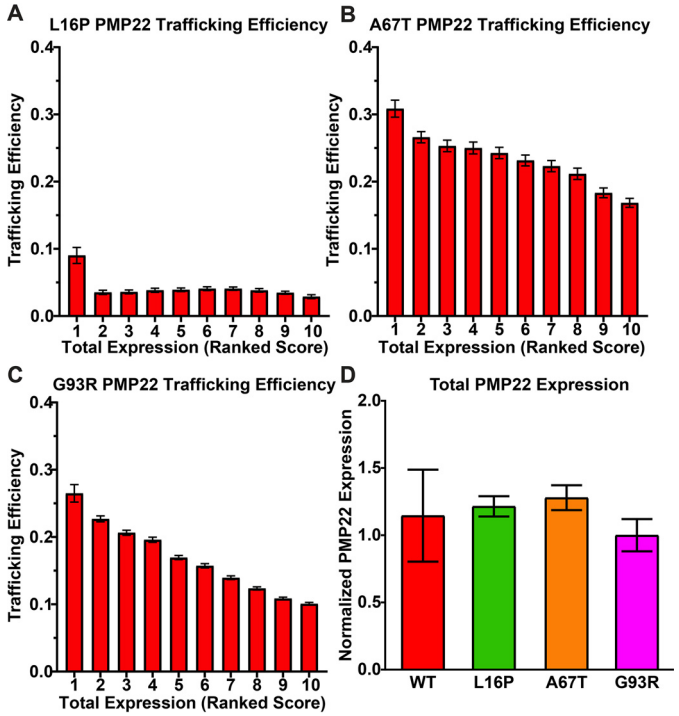

Figure 3. *A–C*, trafficking efficiencies for L16P (*A*), A67T (*B*), and G93R (*C*) were calculated in each of 7500 individual HEK293 cells from three independent biological replicates and placed into 10 bins of 750 based on total PMP22 expression. The mean trafficking efficiency ± 95% CI is plotted for each bin. *D*, the mean total expression ± 95% CI of transiently transfected cells expressing WT, L16P, A67T, and G93R PMP22 from three independent biological replicates is shown normalized to the expression of WT PMP22 in each replicate.

of the PM population remaining constant (MDCK cells) or increasing only between bins 9 and 10 (HEK293 cells). In total, Fig. 2 shows that PMP22 trafficking efficiency decreases as total expression increases. The burden of trapped PMP22 in the cell increases disproportionately relative to the growth of the PM population of the protein.

Trafficking efficiency for PMP22 disease mutants as a function of total expression

Trafficking efficiency *versus* total expression was examined for three disease-causing PMP22 variants: L16P, A67T, and G93R. The L16P mutation, which results in the Trembler-J mouse phenotype, causes severe demyelination and consequent disease. G93R causes moderate demyelination and moderate CMT, whereas A67T causes a mild form of demyelination and a phenotype known as hereditary neuropathy with liability to pressure palsies (1, 6). The trafficking results for these three mutants are shown in Fig. 3 (*A–C*) (see also average total PMP22 expression per bin shown in Fig. S2, *B–D*). Fig. S3 breaks down surface *versus* internal levels of the three mutants as a function of total expression. Fig. 3*D* shows that the average per-cell total expression levels for each mutant and for WT are comparable.

For L16P PMP22, the most precipitous decrease in trafficking efficiency was seen from bin 1 to bin 2 (Fig. 3*A* and Fig. S3, *A* and *B*). This suggests that the pathway for productive folding and trafficking of L16P PMP22 is relatively efficient at very low total expression levels. After bin 1, the surface trafficking efficiency is reduced to roughly 3%, where it remains over a wide range of total expression levels. The data for A67T and G93R (Fig. 3, *B* and *C*, and Fig. S3, *C–F*) is similar to that of WT PMP22 in that the highest trafficking efficiency for these mutants occurs at the lowest levels of total expression, and trafficking efficiency gradually decreases as total expression increases. As for WT, the fractional growth of internal PMP22 population is usually higher than for the PM population at the initial bin 1–to–bin 2 transition and also for the later bins (Fig. S3, *B*, *D*, and *F*).

PMP22 trafficking efficiency under conditions of stable expression

In the above experiments, transient transfection was used to express PMP22 in HEK293 and MDCK cells. This process results in high levels of PMP22 expression. In contrast, stable expressor cell lines, which involve stable integration of plasmid DNA into the host cell genome, generally result in lower protein expression per cell (28). To examine PMP22 trafficking under these conditions, we generated HEK293 cells that stably expressed myc-tagged WT PMP22 (stable cells; Fig. S4).

In Fig. 4*A*, we measured WT PMP22 PM and internal expression in single cells and plotted the population distribution of PMP22 trafficking efficiencies. The mean trafficking efficiency was higher (0.57 ± 0.01), and the population distribution was significantly different ($p < 0.05$) than in transiently transfected cells (distribution compared using a pairwise Kolmogorov–Smirnov test (29)). Fig. 4*B* shows that the average per-cell expression of PMP22 in our stable cell line was significantly lower than in transiently transfected cells. These results further support the idea that lower PMP22 expression leads to higher trafficking efficiency.

We binned WT PMP22 stable cell trafficking data as described above, splitting the data into 10 equal-sized bins based on the total PMP22 expression in each cell (~2200 cells/bin; for average PMP22 expression per bin, see Fig. S5*A*). Fig. 4*C* shows that as total expression increases, there is an initial reduction in trafficking efficiency from ~80% at very low total PMP22 to ~55%, where it remains fairly constant over the remainder of the bins. Fig. S5 (*B* and *C*) shows that from bin 1 to bin 5, there is a major jump in the proportion of internal PMP22 relative to a much smaller increase in the PM population, whereas in later bins both PM and internal populations grow at roughly the same pace.

Discussion

WT PMP22 is overexpressed in the most common form of CMT disease, CMT1A. This has led to interest in the possibility that misfolded, nondegraded, PMP22 is a source of cytotoxicity contributing to disease etiology (13, 23, 24, 30, 31). Here, we examined expression of PMP22 in both transiently transfected model cell lines and in stable cells. It should be considered that PMP22 expression in myelinating Schwann cells may be better modeled by the results from the higher-expressing transiently transfected cells (Fig. 4*B*). In myelinating Schwann cells, PMP22 is expressed at very high levels. *PMP22* is under the

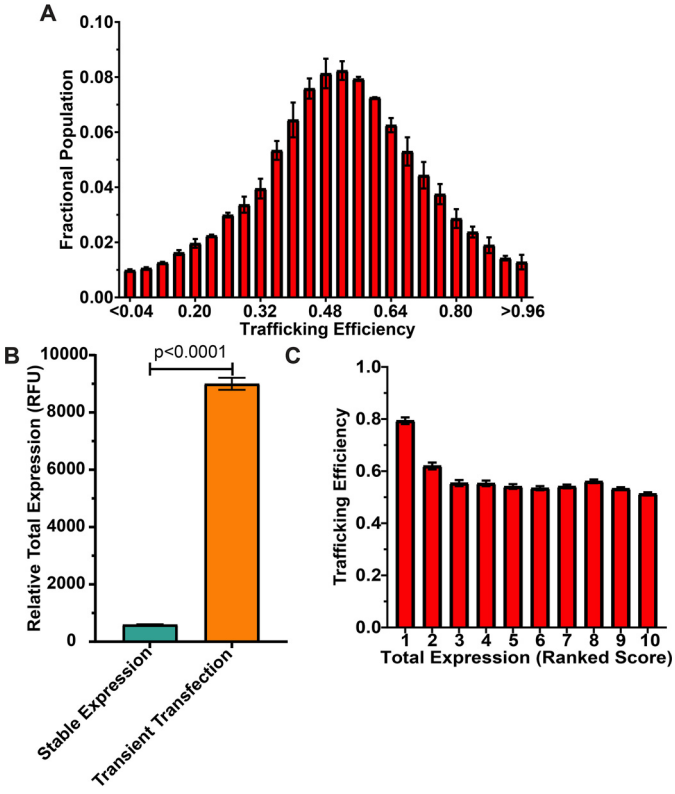

Figure 4. Trafficking efficiency for HEK293 cells stably expressing WT PMP22. *A*, population distribution of WT PMP22 trafficking efficiency measured in individual cells from two independent biological experiments with >11,000 cells measured per replicate. Fractional populations for each bin were calculated for each replicate, and the means ± S.E. are shown. For comparison to transiently transfected HEK293 cells, see Fig. 1*B*. *B*, average total expression (means ± 95% CI) of WT PMP22 (calculated as RFU) in 22,960 individual HEK293 cells stably expressing WT PMP22 from two biological replicates (*aqua*) and 7500 individual HEK293 cells that were transiently transfected (three biological replicates, *orange*). Student's *t* test was used for statistical analysis. Fractional populations for each bin were calculated for each replicate, and the means ± S.E. are shown. *C*, PMP22 trafficking efficiencies for the 22,960 individual WT PMP22 stable expressor cells were placed into 10 bins of 2296 cells each based on total PMP22 expression levels. The mean trafficking efficiency ± 95% CI is plotted for each bin.

control of a powerful transcriptional system that utilizes two promotors, P1 and P2, and a super-enhancer upstream of P1 (7). Most cell types only express transcripts using P2 and consequently express only low levels of PMP22, whereas Schwann cells utilize both promotors to drive higher PMP22 expression. Transcription factor binding and open chromatin markers were found to be much more abundant at the PMP22 super-enhancer in myelinating Schwann cells compared with oligodendrocytes (32). Furthermore, deletion of this super-enhancer in a Schwann cell line dramatically reduced PMP22 transcripts (33). Under conditions of CMT1A trisomy, in which the super-enhancer and promotors are also duplicated, the level of expressed PMP22 may be even higher. We therefore argue that the results in transiently transfected cells are more revealing than the results from stable cells.

Large populations of transiently transfected HEK293 and MDCK cells exhibited average WT PMP22 trafficking efficiencies in the vicinity of 0.20, which is what was previously documented for Schwann cells (19, 20). It is notable that the average trafficking efficiency in MDCK cells (0.17) is lower than in HEK293 cells (0.27). We suggest that this is because the average expression level of PMP22 in MDCK cells is higher than in HEK293 cells, leading to increased misfolding (Fig. 2, *C* and *D*). This is supported by the fact that the trafficking efficiency in stable cells, where average total expression level is significantly lower (Fig. 4*B*), jumps to 0.57. This same trend of lower trafficking efficiency at high expression levels is seen within each population of transiently transfected cells (Fig. 2, *A* and *B*) and to a modest degree in the stable cells (Fig. 4*C*). For both transiently transfected cell lines, a jump is seen in the growth of the internal PMP22 population that is disproportionately higher than for the PM population both at low and high total expression levels (Fig. 2, *E* and *F*). Between the two extremes, the growth of the internal fraction is roughly the same as the PM fraction. This suggests complexity in terms of the cellular PMP22 folding, misfolding, and trafficking processes, complexity that is not hard to imagine given the intricacies of the ER folding quality control system (34). Fig. 2 (*C* and *D*) shows that high-level expression of PMP22 results in a considerable burden of internal protein in cells, consistent with the hypothesis that misfolding of PMP22 and subsequent failure of the misfolded protein to be degraded contributes to CMT1A. Nevertheless, it is also seen that the population of PM PMP22 continues to grow as total expression increases, such that our data are consistent with the possibility that the added expression of WT PMP22 may also result in an aberrant gain of function effect.

The results for mutant forms of PMP22, A67T (mild CMT), G93R (moderate CMT), and L16P (severe CMT) show that the efficiency profile of A67T is similar to that of WT, the profile for G93R is similar to WT (except that the decline in efficiency with increased total expression is more steep), and L16P exhibits dramatically reduced efficiency even at the lowest expression levels, with a further reduction to a low level "basin" occurring as total expression increases (Fig. 3 and Fig. S3). It is interesting that the total amount of internal protein seen for all three of the disease mutants is similar at the highest total expression levels (compare bin 10 in Fig. S3, *A*, *C*, and *E*), whereas the amount of PM protein increases dramatically for L16P < G93R < A67T. This does not imply that the loss of PM protein alone explains the differences in disease severity. CMT disease caused by heterozygous L16P/WT *PMP22* expression (Dejerine–Sottas syndrome) is much more severe than for WT/null patients who suffer from hereditary neuropathy with liability to pressure palsies. The most likely explanation for this is that L16P undergoes misfolding and entrapment early in the secretory pathway of patients and drags some of the WT protein down with it via WT/L16P heterodimerization (30, 35). Consequently, the total loss in both L16P and WT forms of PMP22 is likely greater than occurs in WT/null conditions. Thus, possible toxicity associated with the misfolded/mistrafficked protein may be compounded by the reduction in the surface-trafficked protein, leading to a more severe disease phenotype.

Conclusions

Previous studies have shown that PMP22 trafficking efficiency is related to the stability of its folded structure. Even WT

PMP22 appears to have only marginal conformational stability (18, 36), which helps to explain its modest folding efficiency. Disease mutant forms of PMP22 are even less stable, with mistrafficking and disease severity correlating with the degree of destabilization (17). Aggregates and other misfolded forms of proteins in the ER can be recognized and removed from the ER for degradation via either proteasomal or lysosomal pathways (23, 34). However, if these systems are saturated by an overabundance of misfolded protein, then that protein will accumulate—potentially becoming a source of cytotoxicity. Saturation of the membrane protein quality control machinery appears to occur when PMP22 is overexpressed (37). Here, we explored the relationship between expression levels and surface trafficking efficiency of PMP22. It was found that there was a direct, negative, relationship between expression and trafficking efficiency. Moreover, reduced trafficking efficiency was due more to an increase in internal (likely misfolded) PMP22 at higher total expression levels than to reduced PM trafficking. Although it has yet to be explored in tissue from CMT1A patients, the results of this work support the plausibility that the etiology of CMT1A is related to the accumulation of misfolded PMP22. Moreover, the long-term accumulation of misfolded PMP22 in Schwann cells and/or the weakened efficiency of protein degradation pathways with aging would help to explain why CMT1A is a progressive disorder.

Materials and methods

Materials

HEK293 cells were acquired from ATCC (Manassas, VA, USA). Fix and Perm kits from Invitrogen were used to prepare cells for flow cytometry. The antibodies used in this work were anti-Myc tag (catalog no. 9B11) mouse mAb (PE Conjugate; catalog no. 3739), anti-Myc tag (catalog no. 9B11) mouse mAb (Alexa Fluor 647 conjugate; catalog no. 2233), and anti-Myc tag (9B11) mouse mAb (catalog no. 2276) and were purchased from Cell Signaling Technologies (Danvers, MA, USA).

Cloning

Human cDNA for PMP22 was subcloned into a pIRES2–EGFP mammalian expression vector. QuikChange mutagenesis was used to insert a myc epitope into the second extracellular loop of PMP22 within the pIRES2–EGFP vector and to make the various point mutations used in this study. Plasmids were purified using a GenElute HP plasmid midiprep kit (Sigma–Aldrich).

Cell culture and transfections

HEK293 cells were cultured in Dulbecco's modified Eagle's medium containing 10% fetal bovine serum and 1% pen/strep at 37 °C and 5% CO_2. ~24 h prior to transfection, the cells were plated to be 50–60% confluent at the time of transfection. The cells were transfected using the calcium phosphate methodology, and 6-cm^2 plates were transfected with 1.5 μg of DNA. Transfection medium was removed from cells ~12–15 h post-transfection, the cells were washed with PBS, and fresh culture medium was added to each plate. Transfection efficiencies were routinely >50%.

Single-cell flow cytometry trafficking assay

The experimental workflow is depicted in Fig. S2 and a detailed description of the assay protocol is found in Ref. 17.

Stable cell line generation

HEK293 cells were transfected with WT PMP22 as described above. After removal of the transfection medium, the cells were kept under selective pressure via the addition of 750 μg/ml G418 (Invitrogen) to the culture medium. The medium was changed every other day for 2 weeks until the cells were harvested via trypsinization and resuspended in 300 μl of PBS with 5% fetal bovine serum and placed on ice. Using a FACS Aria III (BD Biosciences, San Jose, CA), single cells were selected based on their scattering area and width profiles and plated in individual wells in a 96-well plate containing growth medium without G418. The cells were grown until confluency and progressively expanded to 6-well plates. The cells that stably expressed myc-tagged WT PMP22 were selected based on analysis via Western blotting.

Statistics

Student's *t* test was used to compare mean values, and the Kolmogorov–Smirnov test was used to compare population distributions. All statistical analysis was performed in GraphPad Prism.

Data availability

All data either are presented in the article, are in the supporting information, or are available from the corresponding author (Charles Sanders, Vanderbilt University, chuck.sanders@vanderbilt.edu) upon request.

Acknowledgments—We thank Arina Hadziselimovic for assistance with cloning and Jonathan Schlebach for use of his original MDCK cell data and critical revisions of the manuscript. Flow cytometry experiments were performed in the Vanderbilt University Medical Center Flow Cytometry Shared Resource.

Author contributions—J. T. M. and C. R. S. data curation; J. T. M. formal analysis; J. T. M. and C. R. S. funding acquisition; J. T. M., B. D. C., and C. R. S. investigation; J. T. M. and C. R. S. visualization; J. T. M. and C. R. S. writing-original draft; J. T. M., B. D. C., and C. R. S. writing-review and editing; B. D. C. methodology; C. R. S. conceptualization; C. R. S. resources; C. R. S. supervision; C. R. S. project administration.

Funding and additional information—This work was supported by National Institutes of Health Grants R01 NS095989 (to C. R. S.) and R01 NS107456 (to B. D. C.). J. T. M. was supported by National Institutes of Health Fellowship F31 NS113494 and National Institutes of Health Training Grant T32 NS00749. The Vanderbilt University Medical Center Flow Cytometry Shared Resource is supported by Vanderbilt Ingram Cancer Center Grant P30

CA68485 and Vanderbilt Digestive Disease Research Center Grant P30 DK058404. The content is solely the responsibility of the authors and does not necessarily represent the official views of the National Institutes of Health.

Conflict of interest—The authors declare that they have no conflicts of interest with the contents of this article.

Abbreviations—The abbreviations used are: CMT, Charcot–Marie–Tooth disease; MDCK, Madin–Darby canine kidney; ER, endoplasmic reticulum; PM, plasma membrane; CI, confidence interval; RFU, relative fluorescent units; PMP22, peripheral myelin protein 22.

References

1. Li, J., Parker, B., Martyn, C., Natarajan, C., and Guo, J. (2013) The PMP22 gene and its related diseases. *Mol. Neurobiol.* **47,** 673–698 CrossRef Medline
2. Jetten, A. M., and Suter, U. (2000) The peripheral myelin protein 22 and epithelial membrane protein family. *Prog. Nucleic Acid Res. Mol. Biol.* **64,** 97–129 CrossRef Medline
3. El-Abassi, R., England, J. D., and Carter, G. T. (2014) Charcot–Marie–Tooth disease: an overview of genotypes, phenotypes, and clinical management strategies. *PM R* **6,** 342–355 CrossRef Medline
4. Morena, J., Gupta, A., and Hoyle, J. C. (2019) Charcot–Marie–Tooth: from molecules to therapy. *Int. J. Mol. Sci.* **20,** 3419 CrossRef Medline
5. Pareyson, D., Saveri, P., and Pisciotta, C. (2017) New developments in Charcot–Marie–Tooth neuropathy and related diseases. *Curr. Opin. Neurol.* **30,** 471–480 CrossRef Medline
6. DiVincenzo, C., Elzinga, C. D., Medeiros, A. C., Karbassi, I., Jones, J. R., Evans, M. C., Braastad, C. D., Bishop, C. M., Jaremko, M., Wang, Z., Liaquat, K., Hoffman, C. A., York, M. D., Batish, S. D., Lupski, J. R., *et al.* (2014) The allelic spectrum of Charcot–Marie–Tooth disease in over 17,000 individuals with neuropathy. *Mol. Genet. Genomic Med.* **2,** 522–529 CrossRef Medline
7. Pantera, H., Shy, M. E., and Svaren, J. (2020) Regulating PMP22 expression as a dosage sensitive neuropathy gene. *Brain Res.* **1726,** 146491 CrossRef Medline
8. Notterpek, L., Ryan, M. C., Tobler, A. R., and Shooter, E. M. (1999) PMP22 accumulation in aggresomes: implications for CMT1A pathology. *Neurobiol. Dis.* **6,** 450–460 CrossRef Medline
9. Li, J. (2017) Caveats in the established understanding of CMT1A. *Ann. Clin. Transl. Neurol.* **4,** 601–607 CrossRef Medline
10. Snipes, G. J., Suter, U., Welcher, A. A., and Shooter, E. M. (1992) Characterization of a novel peripheral nervous system myelin protein (PMP-22/SR13). *J. Cell Biol.* **117,** 225–238 CrossRef Medline
11. Welcher, A. A., De Leon, M., Suter, U., Snipes, G. J., Meakin, S. O., and Shooter, E. M. (1992) Isolation of transcriptionally regulated sequences associated with neuronal and non-neuronal cell interactions. *Prog. Brain Res.* **94,** 163–176 CrossRef Medline
12. Mittendorf, K. F., Marinko, J. T., Hampton, C. M., Ke, Z., Hadziselimovic, A., Schlebach, J. P., Law, C. L., Li, J., Wright, E. R., Sanders, C. R., and Ohi, M. D. (2017) Peripheral myelin protein 22 alters membrane architecture. *Sci. Adv.* **3,** e1700220 CrossRef Medline
13. Lee, S., Bazick, H., Chittoor-Vinod, V., Al Salihi, M. O., Xia, G., and Notterpek, L. (2018) Elevated peripheral myelin protein 22, reduced mitotic potential, and proteasome impairment in dermal fibroblasts from Charcot–Marie–Tooth disease type 1A patients. *Am. J. Pathol.* **188,** 728–738 CrossRef Medline
14. Lee, S., Amici, S., Tavori, H., Zeng, W. M., Freeland, S., Fazio, S., and Notterpek, L. (2014) PMP22 is critical for actin-mediated cellular functions and for establishing lipid rafts. *J. Neurosci.* **34,** 16140–16152 CrossRef Medline
15. Zhou, Y., Miles, J. R., Tavori, H., Lin, M., Khoshbouei, H., Borchelt, D. R., Bazick, H., Landreth, G. E., Lee, S., Fazio, S., and Notterpek, L. (2019) PMP22 regulates cholesterol trafficking and ABCA1-mediated cholesterol efflux. *J. Neurosci.* **39,** 5404–5418 CrossRef Medline
16. Notterpek, L., Roux, K. J., Amici, S. A., Yazdanpour, A., Rahner, C., and Fletcher, B. S. (2001) Peripheral myelin protein 22 is a constituent of intercellular junctions in epithelia. *Proc. Natl. Acad. Sci. U.S.A.* **98,** 14404–14409 CrossRef Medline
17. Schlebach, J. P., Narayan, M., Alford, C., Mittendorf, K. F., Carter, B. D., Li, J., and Sanders, C. R. (2015) Conformational stability and pathogenic misfolding of the integral membrane protein PMP22. *J. Am. Chem. Soc.* **137,** 8758–8768 CrossRef Medline
18. Schlebach, J. P., Peng, D., Kroncke, B. M., Mittendorf, K. F., Narayan, M., Carter, B. D., and Sanders, C. R. (2013) Reversible folding of human peripheral myelin protein 22, a tetraspan membrane protein. *Biochemistry* **52,** 3229–3241 CrossRef Medline
19. Pareek, S., Notterpek, L., Snipes, G. J., Naef, R., Sossin, W., Laliberté, J., Iacampo, S., Suter, U., Shooter, E. M., and Murphy, R. A. (1997) Neurons promote the translocation of peripheral myelin protein 22 into myelin. *J. Neurosci.* **17,** 7754–7762 CrossRef Medline
20. Pareek, S., Suter, U., Snipes, G. J., Welcher, A. A., Shooter, E. M., and Murphy, R. A. (1993) Detection and processing of peripheral myelin protein PMP22 in cultured Schwann cells. *J. Biol. Chem.* **268,** 10372–10379 Medline
21. Fabbretti, E., Edomi, P., Brancolini, C., and Schneider, C. (1995) Apoptotic phenotype induced by overexpression of wild-type gas3/PMP22: its relation to the demyelinating peripheral neuropathy CMT1A. *Genes Dev.* **9,** 1846–1856 CrossRef Medline
22. Nobbio, L., Vigo, T., Abbruzzese, M., Levi, G., Brancolini, C., Mantero, S., Grandis, M., Benedetti, L., Mancardi, G., and Schenone, A. (2004) Impairment of PMP22 transgenic Schwann cells differentiation in culture: implications for Charcot–Marie–Tooth type 1A disease. *Neurobiol. Dis.* **16,** 263–273 CrossRef Medline
23. Fortun, J., Go, J. C., Li, J., Amici, S. A., Dunn, W. A., Jr., and Notterpek, L. (2006) Alterations in degradative pathways and protein aggregation in a neuropathy model based on PMP22 overexpression. *Neurobiol. Dis.* **22,** 153–164 CrossRef Medline
24. Fortun, J., Verrier, J. D., Go, J. C., Madorsky, I., Dunn, W. A., Jr., and Notterpek, L. (2007) The formation of peripheral myelin protein 22 aggregates is hindered by the enhancement of autophagy and expression of cytoplasmic chaperones. *Neurobiol. Dis.* **25,** 252–265 CrossRef Medline
25. Rangaraju, S., Verrier, J. D., Madorsky, I., Nicks, J., Dunn, W. A., Jr., and Notterpek, L. (2010) Rapamycin activates autophagy and improves myelination in explant cultures from neuropathic mice. *J. Neurosci.* **30,** 11388–11397 CrossRef Medline
26. Nicks, J., Lee, S., Harris, A., Falk, D. J., Todd, A. G., Arredondo, K., Dunn, W. A., Jr., and Notterpek, L. (2014) Rapamycin improves peripheral nerve myelination while it fails to benefit neuromuscular performance in neuropathic mice. *Neurobiol. Dis.* **70,** 224–236 CrossRef Medline
27. Liu, N., Yamauchi, J., and Shooter, E. M. (2004) Recessive, but not dominant, mutations in peripheral myelin protein 22 gene show unique patterns of aggregation and intracellular trafficking. *Neurobiol. Dis.* **17,** 300–309 CrossRef Medline
28. Dyson, M. R. (2016) Fundamentals of expression in mammalian cells. *Adv. Exp. Med. Biol.* **896,** 217–224 CrossRef Medline
29. Lampariello, F. (2000) On the use of the Kolmogorov–Smirnov statistical test for immunofluorescence histogram comparison. *Cytometry* **39,** 179–188 Medline
30. Tobler, A. R., Liu, N., Mueller, L., and Shooter, E. M. (2002) Differential aggregation of the Trembler and Trembler J mutants of peripheral myelin protein 22. *Proc. Natl. Acad. Sci. U.S.A.* **99,** 483–488 CrossRef Medline
31. Chittoor-Vinod, V. G., Lee, S., Judge, S. M., and Notterpek, L. (2015) Inducible HSP70 is critical in preventing the aggregation and enhancing the processing of PMP22. *ASN Neuro* **7,** 175909141556990 CrossRef Medline
32. Lopez-Anido, C., Sun, G., Koenning, M., Srinivasan, R., Hung, H. A., Emery, B., Keles, S., and Svaren, J. (2015) Differential Sox10 genomic occupancy in myelinating glia. *Glia* **63,** 1897–1914 CrossRef Medline

33. Pantera, H., Moran, J. J., Hung, H. A., Pak, E., Dutra, A., and Svaren, J. (2018) Regulation of the neuropathy-associated Pmp22 gene by a distal super-enhancer. *Hum. Mol. Genet.* **27,** 2830–2839 CrossRef Medline
34. Marinko, J. T., Huang, H., Penn, W. D., Capra, J. A., Schlebach, J. P., and Sanders, C. R. (2019) Folding and misfolding of human membrane proteins in health and disease: from single molecules to cellular proteostasis. *Chem. Rev.* **119,** 5537–5606 CrossRef Medline
35. Sanders, C. R., Ismail-Beigi, F., and McEnery, M. W. (2001) Mutations of peripheral myelin protein 22 result in defective trafficking through mechanisms which may be common to diseases involving tetraspan membrane proteins. *Biochemistry* **40,** 9453–9459 CrossRef Medline
36. Sakakura, M., Hadziselimovic, A., Wang, Z., Schey, K. L., and Sanders, C. R. (2011) Structural basis for the Trembler-J phenotype of Charcot–Marie–Tooth disease. *Structure* **19,** 1160–1169 CrossRef Medline
37. Fortun, J., Li, J., Go, J., Fenstermaker, A., Fletcher, B. S., and Notterpek, L. (2005) Impaired proteasome activity and accumulation of ubiquitinated substrates in a hereditary neuropathy model. *J. Neurochem.* **92,** 1531–1541 CrossRef Medline